Patterns in natural systems

Sewalt, L.

4

Tumor spread with an Allee effect[1]

4.1 Introduction

4.1.1 Allee effects and tumor growth

A recent article in *Nature Reviews Cancer*, [94], has highlighted how a well-established concept in ecology–the Allee effect [2]–is also relevant to tumors but has yet to be incorporated into their modelling. In its strong form, the Allee effect refers to the observation that there is a population threshold below which a species has negative population growth, driving it to extinction. The weak form of the Allee effect describes a species that has small (but not negative) population growth at low populations [25]. The ecological causes of Allee effects (which are observed within small populations) are multitudinous: the inability to find a mate; the negative impact on co-operative behaviors such as anti-predator vigilance; the increased sensitivity to demographic stochasticity; and, the lack of diversity in the extant gene pool [26, 86, 148]. Evidence for the strong [12, 27, 65, 81, 99] and weak [2, 5, 30, 151, 152] Allee effects are plentiful across many taxa; additional reviews are available in [64, 95]. Consequently, there is a proliferation of mathematical models of the Allee effect in ecology [7, 8, 29, 70, 96, 102, 130, 175, e.g.]. While studies in ecology often worry about factors that might push a threatened species below the (strong) Allee threshold and thereby towards extinction [137, e.g.], an intriguing possibility in cancer research is whether the Allee effect could be harnessed for controlling or negating the growth of cancerous cells [94], consonant with recent experiments in bacteria [146].

[1] The content of this chapter was published as *Influences of Allee effects in the spreading of malignant tumours* in Journal of Theoretical Biology in 2016, see [140].

While seldom stated, hints of the Allee effect are numerous in the cancer research literature. Firstly, at the most anecdotal level, a tumor is only deemed threatening if it is above a certain size, which is an implicit presumption of a strong Allee threshold. More concrete illustrations are available in clinical trials for papillary and follicular thyroid cancers [107], in which risk-of-spread versus initial tumor size figures indicate that the risk is effectively zero until a minimum primary tumor size is reached. Secondly, studies of tumor dormancy suggest the presence of mechanisms such as a restrictive apoptosis/proliferation equilibrium (a cell density at which natural cell death balances new cell production) or a minimum angiogenic potential requirement for blood vessel formation in the tumor [136]. Such biological considerations translate to the inability of the tumor to grow unless a strong Allee threshold is reached. Thirdly, it has been shown experimentally that in the growth of blebs (spherical protrusions forming along the front boundary of tumors), there is a minimum surface tension below which the blebs cannot expand [155]. Since this surface tension is governed by a variety of poorly understood factors such as available myosin [155], the existing microenvironment can be thought of as essentially imposing an Allee effect. Fourthly, [6] and [127] provide evidence of the co-operation between nearby subclones in the early evolution of tumors through the production and exchange of growth factors. Since co-operation is adversely impacted at low populations, tumor cells must–as in ecological systems–encounter the Allee effect. Fifthly, deleterious mutations accumulate more in smaller tumors [94], thereby driving the population to extinction with much higher probability than larger tumors. Sixthly–and at a much broader level–the very fact that cancers depend on genetic heterogeneity, mutations and subsequent evolution [15, 63, 113], pinpoints the necessity of having a large enough gene pool for successful growth, that is, the requirement of an Allee effect[2]. For example, numerical results from a recent integral equation model that models the number of cells in clones with different mutation rates, indicate that there is a threshold genetic mutation rate below which the cancer cells suffer extinction [4]. It is important to note that most evolutionary models of cancer (see the reviews by [113] and [116]) neglect the spatial structure, which is problematic given that tumors are clinically classified depending on their shape [24]. One way of incorporating genetic mutation information within a spatial spreading model is to treat the stochastic mutations as creating an effective strong Allee threshold.

There are a variety of tumor growth models which examine the roles of additional effects such as acidity [53, 111, 13], adhesion [20, 55, 141], non-local interactions [150, 55], cell plasticity in proliferation versus migration [50, 72, 153,

[2]This is stating that genetic diversity produces an implicit Allee effect, different from studies on the impact of a *separately imposed* Allee effect on genetic diversity [172, 173].

110], in a range of tumor types. Most models fall into two classes: those which simulate a network of cells [72, 153], and those which rely of continuum modelling [20, 53, 110, 111, 141, 150, e.g.], although some models that make a connection between the two exist, [10, 46, 122, e.g.]. Very recently, a spatio-temporal tumor cell growth model incorporating micro-environmental influences has been studied. That analysis reveals an Allee effect depending on the cell motility versus local cell density, [14].

4.1.2 A new model for malignant tumor invasion

In light of this emergent viewpoint on the relevance of the Allee effect in cancers, we offer in this manuscript, one of the first (see also [17]) cancer spreading model that explicitly includes the Allee effect. Specifically, we examine how the inclusion of the Allee effect changes conclusions in comparison to the commonly used logistic growth model. For our comparison – the first of its kind – we choose to examine a model of a malignant, solid tumor invading through the extracellular matrix (ECM) via hapto- or chemotaxis, as opposed to the more complex, metastatic dissemination regime [170]. In particular, our analysis applies to the spread of tumors in which hapto- or chemotaxis is the dominant mechanism of cell migration, such as melanoma [109, 125]. We focus on the behavior of the tumors on a long time scale; we do not analyse the transient dynamics.

We assume that an invasive tumor front can be modeled, mathematically, by a traveling wave solution (TWS) with constant speed c. TWSs correspond to stationary solutions in an appropriately moving frame and are defined on a one-dimensional, unbounded spatial domain. While this choice of domain is a simplification of the geometry of tumor invasion, it is a reasonable approximation, while still yielding a model that is amenable to mathematical analysis.

We build on a model of malignant tumor invasion derived in [126] and subsequently studied in [67, 109]. In these articles, a logistic growth term is used to model the growth of the cancer cells (see paragraph 4.1.4); Allee effects are neglected. Here, we replace this logistic growth term with an Allee growth term and study the existence of TWSs of the following dimensionless model for malignant tumor invasion (see section 4.2 for the derivation):

$$\begin{aligned} \frac{\partial u}{\partial t} &= \overbrace{-u^2 w}^{\text{proteolysis}} + \overbrace{\varepsilon\beta \frac{\partial^2 u}{\partial x^2}}^{\text{diffusion}}, \\ \frac{\partial w}{\partial t} &= \underbrace{f(u,w)}_{\text{growth}} - \underbrace{\frac{\partial}{\partial x}\left(\frac{\partial u}{\partial x} w\right)}_{\text{hapto-/chemotaxis}} + \underbrace{\varepsilon \frac{\partial^2 w}{\partial x^2}}_{\text{diffusion}}, \end{aligned} \tag{4.1}$$

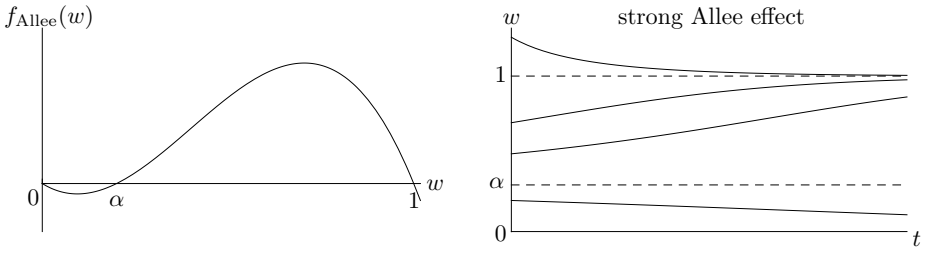

Figure 4.1: Left-hand panel: Sketch of $f_{\text{Allee}} = w(1-w)(w-\alpha)$ for $0 < \alpha < 1$. Observe that $f_{\text{Allee}} > 0$ for $\alpha < w < 1$. Right-hand panel: Sketch of the solutions to $w' = w(1-w)(w-\alpha)$ with $0 < \alpha < 1$. Initial conditions larger than α approach the carrying capacity (which is scaled to one), while initial conditions smaller than α die out out and approach $w = 0$.

with

$$f(u,w) = f_{\text{Allee}}(w;\alpha) \coloneqq w(1-w)(w-\alpha)\,, \quad |\alpha| < 1\,. \tag{4.2}$$

The dependent variables $u \geq 0$ and $w \geq 0$ represent the dimensionless ECM and cancer cell densities, respectively. The independent variables $t > 0$ and $x \in \mathbb{R}$ represent time and one-dimensional space, respectively. Both species are assumed to diffuse slowly, which is modeled by the small parameter ε: $0 \leq \varepsilon \ll 1$. We further assume that the ECM diffuses more slowly than the cancer cells: $0 \leq \beta \leq 1$ and independent of ε. Observe that our analysis is also able to capture the situation of the ECM not diffusing, i.e. $\beta = 0$. The observed migration of the cancer cells up the gradient of ECM is modeled by the hapto- or chemotaxis term. As the cancer cells migrate they break down the ECM; this is modeled by the proteolysis term. The cubic function describing the growth of the cancer cells, (4.2), models the Allee effect, with different values of α corresponding to different strengths. Consistent with the definition in Section 4.1.1, the Allee effect modeled by (4.2) describes the following.

A positive α models the strong Allee effect. Since the carrying capacity of the cancer cell density has been scaled to one in (4.2), we require $\alpha < 1$. The strong Allee effect imposes a growth threshold on the tumor, whereby the cancer cell population only increases (at a given location) if $\alpha < w < 1$, since otherwise $f_{\text{Allee}} \leq 0$. See also Figure 4.1. In the context of tumor invasion, $\alpha \gtrapprox 0$ is the most appropriate representation of the strong Allee effect as it is unlikely that a large threshold value (relative to the carrying capacity) is needed for the proliferation of cancer cells.

A negative α models the weak Allee effect. Unlike the strong Allee effect,

the weak Allee effect does not impose a growth threshold. Instead, it models a population with a growth rate that is initially positive and increases with population increase for *small* populations, until crowding effects take over and cause the growth rate to decrease with further population increase. Hence, we require $\alpha > -1$, with $\alpha \gtrapprox -1$ corresponding to the most appropriate representation of the weak Allee effect. For further discussion and more precise definitions of the strong and weak Allee effects, see [25] and Appendix A.

4.1.3 Main results

The focus of this chapter is to compare the Allee model (4.1)–(4.2) with the logistic model, developed in [126], with respect to its ability to capture the behavior of malignant tumor invasion. Furthermore, we compare our results to a different modification of the logistic model, studied in [108], where competition between the species is included in $f(u, w)$ in (4.1). For convenience, we refer to (4.1)–(4.2) with $\alpha \gtrapprox 0$ and $\alpha \gtrapprox -1$ as the strong and weak Allee models, respectively. We present evidence that the strong Allee model provides a better model of tumor invasion than these previously proposed models, while the weak Allee model provides no significant improvement. The following sections provide a summary of the main results that lead to these conclusions.

Strong Allee model

For the strong Allee model, we find that:

- Only invasive tumor fronts with well-defined edges [108] (so-called *Type III waves*, see Section 4.1.4) exist, rather than the whole family that exists for the previously studied models of malignancies such as melanoma [67, 108, 109, 126]; and,

- A non-monotonic (biphasic) relationship between the background ECM density and the invasion speed of the tumor is evident, consistent with the experiments on a HT1080 fibrosarcoma cell line invading collagen gels as reported in [125, 108]. In contrast, models without the Allee effect predict a monotonic relationship [67, 126, 109]. See in particular Figure 11 in [67].

These results are illustrated in Figure 4.2. The numerical method used to simulate (4.1)–(4.2) uses a vertex-centered finite volume discretisation in space, with upwinding to approximate u and w at the faces of the control volumes, on a linear mesh with $\Delta x = 1/80$. The resultant ODEs are integrated in time using `MATLAB`'s inbuilt ODE solver `ode45` (which uses a variable-order Runge–Kutta algorithm with adaptive timestepping).

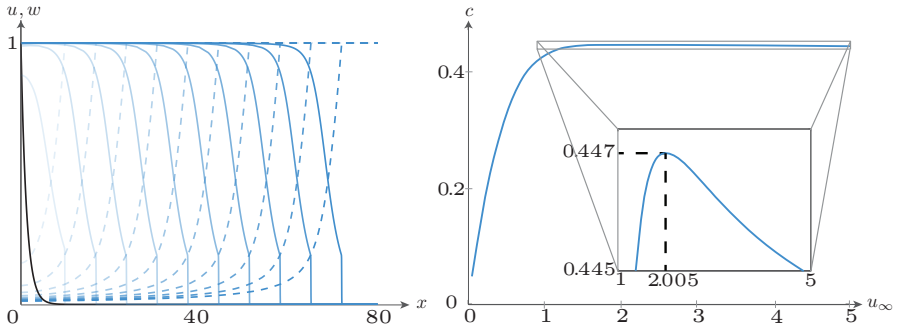

Figure 4.2: Left-hand panel: A *Type III wave* with a biologically justified, well-defined edge and speed $c \approx 0.43$, obtained by numerically simulating (4.1)–(4.2) with $\varepsilon = 0.001$, $\alpha = 0.05$ and $\beta = 0.5$. The dashed lines correspond to u-profiles and the solid lines to w-profiles, with solutions plotted at $t = 0$ (black), 16 (lightest), $32, \ldots, 160$ (darkest). Right-hand panel: The leading order ($\varepsilon = 0$) component of the speed of traveling wave solutions of (4.1)–(4.2) (c) versus the background ECM density (u_∞), with $\alpha = 0.05$, illustrating a biphasic relationship.

Weak Allee model

In contrast, the main result relating to the weak Allee model is that it offers no notable benefits over the previously studied models for tumor invasion such as melanoma and, so, due to its added complexity, is a less preferable model of malignant invasion. Consequently, we omit the derivation of the results from the main body of the chapter; we present them briefly in Appendix B. The key findings that lead to our conclusion are as follows.

- There exists a family of invasive tumor fronts (so-called *Type I–IV waves*), which includes some that have non-sharp fronts but that appear (numerically) to be stable and, hence, observable within the system.
- The relationship between the background ECM density and the invasion speed of the tumor fronts with sharp edges is monotonically increasing, contrary to an experimentally observed biphasic relationship [125].

4.1.4 Comparison with results for previous models

In the models for malignant tumor invasion studied in [67, 109, 125, 126], the cancer cells are assumed to grow logistically, governed by the dimensionless

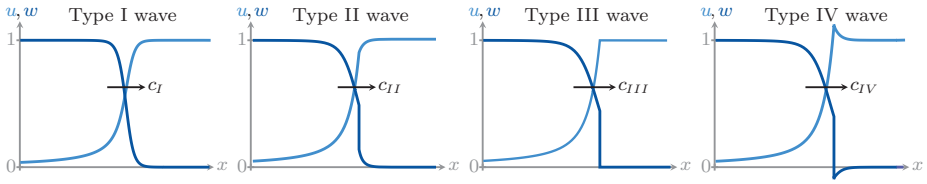

Figure 4.3: Schematics of the four types of traveling wave solutions discussed in this chapter. This figure is an adaptation of Figure 6 in [67]. Copyright ©2014 Society for Industrial and Applied Mathematics. Reprinted with permission. All rights reserved.

kinetic function

$$f(u,w) = f_{\text{logistic}}(w) \coloneqq w(1-w)\,. \tag{4.3}$$

In the model studied in [108], an interaction term between the ECM (u) and cancer cells (w) is added to (4.3) to signify the competition for space between the two species. Subsequently, the growth of the cancer cells is governed by the dimensionless kinetic function

$$f(u,w) = f_{\text{competition}}(w) \coloneqq w(1-w) - \gamma uw\,. \tag{4.4}$$

Thus, the models studied previously are (4.1), with (4.3) or (4.4) in place of (4.2)[3]. Henceforth, for convenience, we refer to the former as the logistic model and the latter as the competition model.

In [67], it is shown that the logistic model admits a continuous family of traveling wave solutions (TWSs). This family is classified into four distinct types, according to qualitative differences in the cancer cell density profiles, in the singular limit $\varepsilon \to 0$; see Figure 4.3. A *Type I wave* has a smooth, exponentially decaying cancer cell density profile. A *Type II wave* has a cancer cell density profile with a shock but that remains positive and decays exponentially to zero as $x \to \infty$. A *Type III wave* has a cancer cell density profile with a shock and semi-compact support. A *Type IV wave* has a cancer cell density profile with a shock and that decays exponentially to zero as $x \to \infty$ but with densities that are negative after the shock. Preliminary numerical results suggest that the Type I–III waves are stable, in the sense that they are observable in the system, while the Type IV waves are not [67].

Remark 4.1. The labelling of the four wave types depicted in Figure 4.3 refers to those waves identified in [67] for the logistic model. However, the classifications

[3] In [109, 126, 108], it is assumed, for simplicity, that $\varepsilon = 0$. In [67], $\beta = 1$.

that underpin this terminology apply more generally, for example, to TWSs of (4.1) with $0 \leq \varepsilon \ll 1$ and $0 \leq \beta \leq 1$. Thus, we adopt the labels Type I–IV and henceforth use them to refer to any waves with equivalent features to those described in [67], outlined above.

A similar family of Type I–IV waves exists for the competition model, studied in [108][4]. Moreover, numerical simulations suggest that in certain, broad parameter regimes, the Type I–III waves are stable and, hence, observable in the system. Although the Type IV solution is not observable and a negative density has no interpretation in the current application of system (4.1), we consider this type of solution for the sake of completeness.

From a biological perspective, Type III waves are considered to be most realistic for tumors which are expected to posess a well-defined edge; such as melanomas, see for example [108]. In contrast to the logistic, competition and weak Allee models, the strong Allee model automatically *selects* tumors with sharply defined edges.

In [125], a *biphasic relationship* between the background collagen (the predominant ingredient in ECM) density and the invasion speed of malignant tumors is observed experimentally. These experimental results indicate that the invasion speeds of malignant tumors do not increase monotonically with the background collagen (and, hence, ECM) density. Instead, there is some critical density up to which the invasion speed increases but over which the invasion speed decreases. The competition model was proposed in [108] to mathematically replicate this biphasic relationship, which is not a feature of the logistic model [67, 109, 108]. The logistic model exhibits a monotonically increasing relationship between the speed of the Type III waves c_{III} and the background ECM density u_∞, similar to the weak Allee model. By studying only the Type III waves, the desired biphasic relationship is revealed in [108]. Mathematically, this result is facilitated by the existence to two Type III waves, with different u_∞, for certain, fixed speeds.

4.1.5 Outline

The remainder of the chapter is set out as follows. In Section 4.2, we derive the dimensionless model (4.1) from a dimensional model for malignant tumor invasion proposed in [126]. In Section 4.3, we set up the mathematical framework that is required to prove the main results of the strong Allee model, described in Section 4.1.3. We prove (in a mathematically rigorous way) that the strong Allee model only admits Type III traveling wave solutions. The framework we follow exploits the separation of scales between the hapto- or chemotaxis and diffusion terms. It is based on that described in [167] and uses geometric singular perturbation

[4]Only Type III waves are considered in [108] but, using methods developed in [167] and used in [67] and here, it can be shown that Type I, II and IV waves also exist.

theory (GSPT) [73, 82, 84] and canard theory [11, 97, 149, 166]. The results for the strong Allee model are further analysed in Section 4.4, including the biological implications of our findings in relation to previously studied models. In Section 4.5, we discuss the extension of our results to a more general class of models, the limitations of our work and topics for future research.

Remark 4.2. The mathematical derivation contained within Section 4.3 is not prerequisite to following the arguments and discussions contained within the subsequent sections. Thus, we invite the less mathematically inclined reader to skip over it.

4.2 Model derivation

Our decision to study (4.1) is inspired by [126], where, after a quasi-steady state approximation, the following dimensional model of malignant tumor invasion is studied (using the notation in [67]):

$$\begin{aligned} \frac{\partial \hat{u}}{\partial \hat{t}} &= -k_4 \hat{u}^2 \hat{w}, \\ \frac{\partial \hat{w}}{\partial \hat{t}} &= \hat{k}_1 \hat{w}(k_2 - \hat{w}) - k_3 \frac{\partial}{\partial \hat{x}} \left(\frac{\partial \hat{u}}{\partial \hat{x}} \hat{w} \right), \end{aligned} \tag{4.5}$$

Here, $\hat{x}$ represents one-dimensional space (in metres, m) and $\hat{t}$ represents time (in seconds, s). The dependent variable $\hat{u}$ (kg m^{-3}) represents the ECM density and $\hat{w}$ (cells m^{-3}) represents the cancer cell density. Diffusion of the species is assumed to be small and therefore neglected. The parameter $k_3 > 0$ (m^5 kg^{-1} s^{-1}) measures the strength of the hapto- or chemotaxis term, which models the observed migration of cancer cells up the gradient of ECM. The nonlinear function $-k_4 \hat{u}^2 \hat{w}$ models the degradation of the ECM via proteolysis at rate $k_4 > 0$ (m^6 kg^{-1} cells^{-1} s^{-1})[5]. The proliferation of the cancer cells is modeled by the nonlinear function $\hat{k}_1 \hat{w}(k_2 - \hat{w})$: without spatial influences and independent of the other species, the cancer cells grow logistically to their carrying capacity $k_2 > 0$ (cells m^{-3}), with (constant) proliferation rate $\hat{k}_1 k_2 > 0$ (s^{-1}). We refer to [126] for a more detailed derivation of (4.5).

We wish to study the influence of incorporating an Allee effect into the description of the growth of the cancer cells. We assume the same nonlinearity for proteolysis but replace the cancer cell growth function with an Allee term. Following [167], we reintroduce the small amount of diffusion of both the ECM

[5] An enzyme–protease–that is produced in the presence of cancer cells, breaks down the ECM in a process called proteolysis. However, the protease reaction evolves on a much faster time scale than the other processes within the tumor and so a quasi-steady state reduction is applied; see [126] for more details.

and cancer cells that was neglected in (4.5). With these adaptations, the model under investigation becomes

$$\begin{aligned}\frac{\partial \hat{u}}{\partial \hat{t}} &= -k_4 \hat{u}^2 \hat{w} + D_1 \frac{\partial^2 \hat{u}}{\partial \hat{x}^2},\\ \frac{\partial \hat{w}}{\partial \hat{t}} &= k_1 \hat{w}(k_2 - \hat{w})(\hat{w} - k_6) - k_3 \frac{\partial}{\partial \hat{x}} \left(\frac{\partial \hat{u}}{\partial \hat{x}} \hat{w} \right) + D_2 \frac{\partial^2 \hat{w}}{\partial \hat{x}^2},\end{aligned} \tag{4.6}$$

with $k_i > 0$ for $i \in \{1, \ldots, 5\}$, $|k_6| < k_2$ and $0 \leq D_1 \leq D_2$ ($\mathrm{m}^2\ \mathrm{s}^{-1}$). We will allow for the ECM to have both no diffusion ($D_1 = 0$), and small diffusion, in comparison to the cancer cells.

Here, k_2 (cells m^{-3}) is still the carrying capacity of the cancer cell density, while $k_1 k_2 k_6 (\hat{w}/k_6 - 1)$ (s^{-1}) is the (density dependent) proliferation rate. This density dependent proliferation rate, in contrast to the constant proliferation rate assumed by logistic growth, is the main difference between the two models, (4.5) and (4.6). For $k_6 > 0$, k_6 (cells m^{-3}) represents a growth threshold, below which the cancer cell density decreases, consistent with the strong Allee effect. For $k_6 < 0$, the interpretation of k_6 is less clear. However, the effect of the term $(1 + \hat{w}/(-k_6))$ is to increase the proliferation rate, relative to the (constant) rate $k_1 k_2 (-k_6)$, with this increase more pronounced as the cancer cell density increases, consistent with the weak Allee effect; see [25] for further discussion of the weak (and strong) Allee effects and their mathematical representation.

We introduce

$$u = \frac{\hat{u}}{U}, \quad w = \frac{\hat{w}}{W}, \quad t = \frac{\hat{t}}{T}, \quad x = \frac{\hat{x}}{X}, \tag{4.7}$$

with

$$U = \frac{k_1 k_2}{k_4}, \quad W = k_2, \quad T = \frac{1}{k_1 k_2^2}, \quad X = \sqrt{\frac{k_3}{k_2 k_4}},$$

and define

$$\alpha := \frac{k_6}{k_2} < 1, \quad \beta := \frac{D_1}{D_2} \leq 1, \quad \varepsilon := \frac{k_4}{k_1 k_2 k_3} D_2.$$

This nondimensionalisation transforms (4.6) to (4.1)–(4.2), restated here for convenience:

$$\begin{aligned}\frac{\partial u}{\partial t} &= -u^2 w + \varepsilon \beta \frac{\partial^2 u}{\partial x^2},\\ \frac{\partial w}{\partial t} &= w(1 - w)(w - \alpha) - \frac{\partial}{\partial x} \left(\frac{\partial u}{\partial x} w \right) + \varepsilon \frac{\partial^2 w}{\partial x^2},\end{aligned} \tag{4.8}$$

with $(x,t) \in (\mathbb{R}, \mathbb{R}^+)$, $|\alpha| < 1$, $0 \leq \beta \leq 1$ and $0 < \varepsilon \ll 1$. The new variables u, w, x and t, and parameters α, β and ε are dimensionless; see Appendix C. Moreover, α and β are assumed to be $\mathcal{O}(1)$ with respect to ε: (loosely speaking) for $\alpha, \beta > 0$ they are independent of ε and do not approach zero in the limit $\varepsilon \to 0$. Due to the choice of nondimensionalisation, the carrying capacity of the cancer cells has been scaled to one and the strength of the Allee effect is solely measured by the parameter α.

The significant reduction in the number of parameters from eight in (4.6) to three in (4.8) makes the latter (dimensionless) model considerably more amenable to mathematical analysis.

4.3 Type III traveling wave solutions

In this section, we provide the mathematical foundation to derive the results for the strong Allee model ((4.8) with $\alpha \gtrapprox 0$, $0 \leq \beta \leq 1$ and ε sufficiently small), stated in Section 4.1.3. We prove that this model only admits Type III traveling wave solutions (TWSs).

In the strong Allee model the homogeneous equilibria $(u,w) = (0,1)$ and $(u_\infty, 0)$, with $u_\infty \in \mathbb{R}$, represent an all-cancer state and a cancer-free state, respectively. When studying invasive tumor fronts, we are interested in connections between these two states. From a mathematical standpoint, we study the existence of right-moving TWSs of (4.1)–(4.2) that travel with constant speed: $c > 0$. Such solutions correspond to stationary solutions in the moving frame $z = x - ct$ and so satisfy

$$\begin{aligned} -cu_z &= -u^2 w + \varepsilon \beta u_{zz}\,, \\ -cw_z &= w(1-w)(w-\alpha) - (u_z w)_z + \varepsilon w_{zz}\,, \end{aligned} \tag{4.9}$$

TWSs also satisfy the asymptotic boundary conditions

$$\lim_{z \to -\infty} (u,w) = (0,1)\,, \quad \lim_{z \to \infty} (u,w) = (u_\infty, 0)\,, \quad u_\infty \in \mathbb{R}^+\,, \tag{4.10}$$

where u_∞ represents the (variable) background ECM density, as in [67]. Thus, TWSs of (4.1)–(4.2) or (4.8) correspond to heteroclinic connections of (4.9) that satisfy (4.10).

Theorem 4.3.1. *For $0 < \varepsilon \ll 1$ sufficiently small and $0 < \alpha < 1$, $0 \leq \beta \leq 1$ and $\mathcal{O}(1)$ with respect to ε, the only possible solution of (4.9)–(4.10) corresponds to a Type III traveling wave solution of* (4.1)–(4.2).

We prove Theorem 4.3.1 using a method outlined in [167], which was subsequently used in [67] to study the logistic model. The foundation of this method

lies in geometric singular perturbation theory (GSPT) [73, 82, 84], which provides a geometric approach to singular perturbation problems. The benefit of using GSPT lies in the rigorous theory that underpins it, which exploits the geometric structure embedded in models such as (4.1) and allows us to prove that the leading order solutions we construct are good approximations of the full solutions with $0 < \varepsilon \ll 1$. Canard theory [11, 97, 149, 166] is also used when the standard GSPT, known as Fenichel theory [49, 82], becomes invalid due to a loss of normal hyperbolicity of the critical manifold. Conditions on the vector field of (4.9) that guarantee the existence of Type III TWSs are also derived.

4.3.1 Set-up

System (4.9) is singularly perturbed, due to the different asymptotic scalings of the diffusion and hapto- or chemotaxis terms, with perturbation parameter $0 \leq \varepsilon \ll 1$. Singularly perturbed systems exhibit an inherent separation of scales. In Figures 4.2 and 4.3, for example, we observe two spatiotemporal scales: the *fast scale* captures the dynamics where rapid changes occur, which, in the singular limit, correspond to shocks in the solutions; and, the *slow scale* relates to the dynamics away from the shocks (in the singular limit), or where less rapid changes occur.

The separation of slow and fast behavior becomes more evident when we write the w-equation of (4.9) as a balance law

$$(\varepsilon w_z - u_z w + cw)_z = -w(1-w)(w-\alpha).$$

So, we define two new variables,

$$p \coloneqq u_z \quad \text{and} \quad v \coloneqq \varepsilon w_z - pw + cw\,,$$

(see [67] and [167] for a further rationale behind the rescaling above). This way, we can write (4.9) as a four-dimensional system of first-order ordinary differential equations (ODEs):

$$\begin{aligned} u_z &= p\,, \\ v_z &= -w(1-w)(w-\alpha)\,, \\ \varepsilon p_z &= \frac{1}{\beta}(u^2 w - cp)\,, \\ \varepsilon w_z &= v + (p-c)w\,. \end{aligned} \tag{4.11}$$

For $\beta = 0$, the equation for p in (4.11) becomes singular. This has to do with the fact that the u-equation of (4.9) is only first order for $\beta = 0$, as opposed to second order for $\beta > 0$. We assume from now on that $\beta > 0$, and discuss

the proof of Theorem 4.3.1 for $\beta = 0$ (which goes along the same lines as for $\beta > 0$) in some more detail in Remark 4.4. Following standard terminology from geometric singular perturbation theory (see for example [82, 84]) we label (4.11) the *slow system*, with z the *slow traveling wave coordinate*. Provided $\varepsilon \neq 0$, we can equivalently write (4.11) in terms of the fast scale by introducing the *fast traveling wave coordinate*, $y = z/\varepsilon$:

$$\begin{aligned} u_y &= \varepsilon p\,, \\ v_y &= -\varepsilon w(1-w)(w-\alpha)\,, \\ p_y &= \frac{1}{\beta}(u^2 w - cp)\,, \\ w_y &= v + (p-c)w\,. \end{aligned} \tag{4.12}$$

So, (u, v) are the slow variables and their equations determine the dynamics away from the shock, while the equations for the fast variables (p, w) determine the dynamics around the shock. While (4.11) and (4.12) are equivalent for $\varepsilon \neq 0$, in the singular limit $\varepsilon \to 0$, they reduce differently depending on the spatiotemporal scale. In Section 4.3.2–4.3.3, we study the singular limits of (4.12) and (4.11), respectively. The results of these sections determine the leading order behavior of the heteroclinic connections in the appropriate regimes. In Section 4.3.4, the results from Section 4.3.2–4.3.3 are combined to prove Theorem 4.3.1.

4.3.2 Layer problem

On the fast scale, taking the singular limit ($\varepsilon \to 0$) of the so-called *fast system*, (4.12), yields a two-dimensional ODE system, termed the *layer problem*:

$$\begin{aligned} p_y &= \frac{1}{\beta}(u^2 w - cp), \\ w_y &= v + (p-c)w, \end{aligned} \tag{4.13}$$

with two parameters $u, v \in \mathbb{R}$. Since u and v are parameters in (4.13), they remain constant along any shocks in the TWSs of (4.1)–(4.2) with $\varepsilon = 0$.

The equilibria of (4.13) form a two-dimensional surface in (u, v, p, w)-space, referred to as the *critical manifold*, which can be represented as a graph over the original variables (u, w):

$$S := \left\{ (u, v, p, w) \;\middle|\; v = \left(c - \frac{u^2 w}{c}\right) w\,, \quad p = \frac{u^2 w}{c} \right\}. \tag{4.14}$$

The left-hand panel of Figure 4.4 shows a projection of S into (u, v, w)-space.

Lemma 4.3.2. *The critical manifold S is folded around the so-called* fold curve*,*

$$F := \{(u, w) \mid 2u^2 w - c^2 = 0\}\,. \tag{4.15}$$

In other words, at F, two branches of equilibria $(p_\pm(u, v; c), w_\pm(u, v; c))$ of (4.13) *originate in a saddle-node bifurcation, see for example [98] for the conditions of a saddle-node bifurcation. The equilibria $(p_-(u, v),\ w_-(u, v))$ are unstable, or repelling, with respect to* (4.13) *and, hence, we label this branch of S as S_r. The other branch of S, given by $(p_+(u, v; c), w_+(u, v; c))$, is stable, or attracting, and is labelled S_a. S is symmetric in w around F with $w_- \geq w_+$.*

Proof. The proof follows from [167], and is similar to the proof of Lemma 2.2 in [67]; we refer to these works for the details. Briefly: the folded structure of S follows from checking that the standard conditions for a saddle-node (SN) bifurcation are met [98, e.g.]; the stabiltiy of S is evident from the eigenvalue structure of the linearisation of (4.13); and, the symmetry is a consequence of the definition of S. □

The folded structure of S allows heteroclinic connections between S_r and S_a. Such a connection transports a point (u_-, v_-, p_-, w_-) on S_r to the point (u_+, v_+, p_+, w_+) on S_a, with $u_+ = u_-$ and $v_+ = v_-$ (since u and v are constant in (4.13)), and

$$\begin{aligned} p_+ &= \frac{u_-^2 w_+}{c} = c - p_-\,, \\ w_+ &= \frac{c^2}{u_-^2} - w_- = 2F(u_-) - w_-\,. \end{aligned} \tag{4.16}$$

These conditions follow from the definition of S and are equivalent to the Rankine–Hugoniot and Lax entropy conditions for shocks for the strictly hyperbolic system (4.1)–(4.2) with $\varepsilon = 0$; see [67, 109, 167]. The second equation in (4.16) highlights the symmetry of S around F. The right-hand panel of Figure 4.4 provides a schematic of S and an example heteroclinic connection between S_r and S_a via the dynamics of (4.13).

4.3.3 Reduced problem

On the slow scale, taking the singular limit of (4.11) yields a differential–algebraic system with two ODEs coupled to two algebraic constraints, termed the

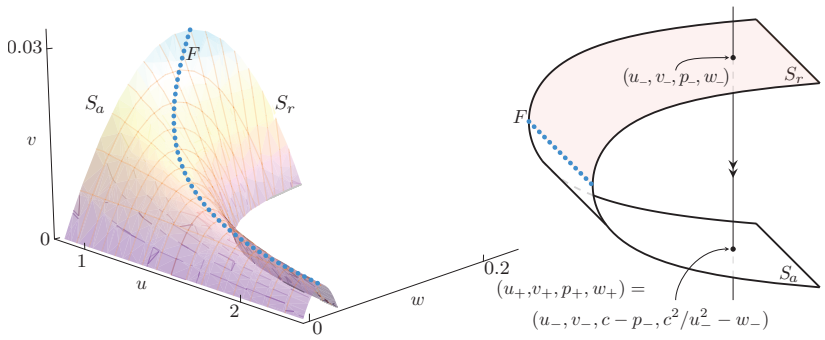

Figure 4.4: The critical manifold S, defined in (4.14). S is folded around the fold curve F, defined in (4.15) and represented by the blue dotted line. It is symmetric in w around F, with one repelling side (S_r) and one attracting side (S_a). Left-hand panel: Projection of the S into (u, v, w)-space, highlighting the folded structure. Right-hand panel: A schematic of S and an example of a flow connecting a point on S_r to the corresponding point on S_a. This is an adaptation of Figure 4 in [68].

reduced problem:

$$\begin{aligned} u_z &= p, \\ v_z &= -w(1-w)(w-\alpha), \\ 0 &= \frac{1}{\beta}(u^2 w - cp), \\ 0 &= v + (p-c)w. \end{aligned} \tag{4.17}$$

As expected from geometric singular perturbation theory, the algebraic constraints define S. Herein lies the geometric structure of the model. When viewed on the slow scale, the flow along S is evident and governed by (4.17).

Since S is given as a graph over the original model variables (u, w), we restrict our investigation of (4.17) to these coordinates, where the slow behavior is governed by

$$\begin{aligned} u_z &= \frac{u^2 w}{c}, \\ \left(c - \frac{2u^2 w}{c}\right) w_z &= -w(1-w)(w-\alpha) + \frac{2u^3 w^3}{c^2}. \end{aligned} \tag{4.18}$$

Consequently, the analysis of the reduced dynamics reduces to a two-dimensional, (u, w)-phase plane analysis. In this projection, the phase space consists of two distinct regions corresponding to S_{a} and S_{r}, separated by F; see, for example, Figure 4.8.

The equilibria of (4.18) in the first quadrant are

$$(u_\infty, 0)\,, \quad (0, \alpha)\,, \quad (0, 1)\,, \quad u_\infty \in \mathbb{R}^+\,.$$

The stability of these equilibria is determined via the associated Jacobian matrix, appended with a perturbation analysis in the case of a zero eigenvalue:

- $(u_\infty, 0)$ has an unstable eigenvalue and a zero eigenvalue (related to the translation in the u direction);
- $(0, \alpha)$ has a stable eigenvalue with eigenvector pointing in the direction of the invariant w-axis and center-unstable outgoing trajectories, directed into the first quadrant; and,
- $(0, 1)$ has an unstable eigenvalue with eigenvector pointing in the direction of the invariant w-axis and center-unstable outgoing trajectories, directed into the first quadrant.

System (4.18) is singular along F, because the left-hand side of the w-equation vanishes here. In general, solution trajectories approaching F have w-derivatives that blow-up in finite time. The isolated points on F at which the right-hand side of (4.18) also vanishes, referred to as *canard points* [11, 166], form the exception to this rule.

To understand solution trajectories of (4.18) interacting with these canard points, we introduce a new variable $\bar{z}$, defined via

$$\frac{\mathrm{d}z}{\mathrm{d}\bar{z}} = c - \frac{2u^2 w}{c}\,.$$

With this change of coordinate system, (4.18) transforms to the so-called *desingularised system*

$$\begin{aligned} \frac{\mathrm{d}u}{\mathrm{d}\bar{z}} &= \frac{u^2 w}{c}\left(c - \frac{2u^2 w}{c}\right)\,, \\ \frac{\mathrm{d}w}{\mathrm{d}\bar{z}} &= -w(1-w)(w-\alpha) + \frac{2u^3 w^3}{c^2}\,. \end{aligned} \tag{4.19}$$

This system is more amenable to analysis than (4.18) as it is no longer singular. Canard points of (4.18) correspond to equilibria of (4.19) on F. They are

classified according to the nature of the corresponding equilibrium in (4.19). For example, if (4.19) has a saddle equilibrium on F, then the corresponding canard point of (4.18) is called a *folded saddle canard point* (FS). Similarly, we have *folded focus canard points* (FF), *folded node canard points* (FN), *etc.*. Two trajectories of a system with a FS can pass through F at such a canard point, thereby flowing from S_a to S_r and *vice versa* [166]. The former trajectory is labelled the *canard solution* and the latter the *faux canard solution*. Trajectories are not able to pass through F at a FF, while a *funnel* of trajectories pass through F at a FN [165, 166]. Figure 4.5 provides a schematic of a FS, FF and FN and illustrates their connection with regular equilibria.

Remark 4.3. The flows of (4.18) and (4.19) differ only in their parametrization. The flows are topologically equivalent in forward $\bar{z}$ if $\mathrm{d}z/\mathrm{d}\bar{z} > 0$ and topologically equivalent in backward $\bar{z}$ if $\mathrm{d}z/\mathrm{d}\bar{z} < 0$. It is straightforward to see that $\mathrm{d}z/\mathrm{d}\bar{z} = c^2 - 2u^2 w < 0$ on S_r, or above F in the (u, w)-plane, while $\mathrm{d}z/\mathrm{d}\bar{z} = c^2 - 2u^2 w > 0$ on S_a, or below F in the (u, w)-plane. Thus, the (u, w)-phase plane of (4.18) is obtained from the (u, w)-phase plane of (4.19) by reversing the direction of the trajectories on S_r, or above F in the (u, w)-plane; see Figure 4.8 for an illustration.

Lemma 4.3.3. *For* $0 < \alpha < 1$, (4.18) *has two canard points if* $0 < c < c^+(\alpha)$, *and no canard points otherwise, where*

$$c^+ = c^+(w^+(\alpha), \alpha) \coloneqq 2\sqrt{2w^+}\left(1 - 2w^+ + \alpha\right) \tag{4.20}$$

and

$$w^+ = w^+(\alpha) \coloneqq \frac{1}{6}\left(1 + \alpha + \sqrt{(1+\alpha)^2 + 12\alpha}\right).$$

The w*-components of both canard points are larger than* α *and smaller than* 1.

Proof. Canard points of (4.18) correspond to equilibria of (4.19) on F. The w-components of these equilibria are real positive roots of

$$q(w) \coloneqq \sqrt{2}(1-w)(w-\alpha) = c\sqrt{w} =: s(w)\,, \tag{4.21}$$

and the corresponding u-components are given by $u = c/\sqrt{2w}$. The number of solutions to (4.21) changes in a saddle-node (SN) bifurcation as $q(w)$ and $s(w)$ become tangent, which occurs at $c = c^+(\alpha)$. From the shapes of the graphs of $q(w)$ and $s(w)$ (parabolic and monotonically increasing, respectively) for different values of c, it follows that the smaller root of (4.21) lies between α and $w^+(\alpha)$, while the larger root lies between $w^+(\alpha)$ and 1. As $c \to 0$, the roots approach α and 1, and as $c \to c^+(\alpha)$, they approach $w^+(\alpha)$. □

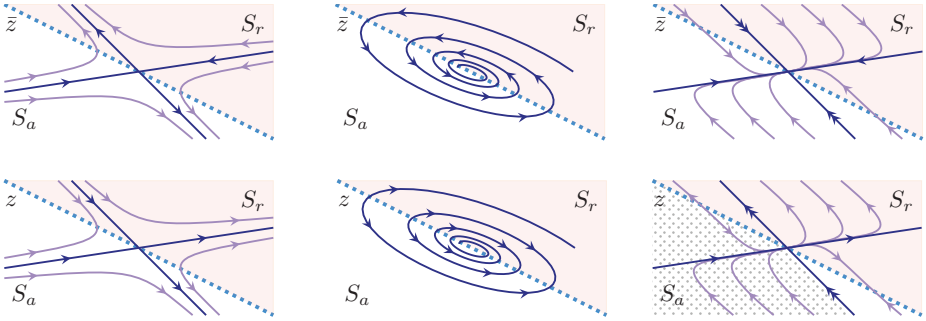

Figure 4.5: Schematics of some types of canard points. The blue dotted line represents F, the upper-right, shaded region S_{r} and the lower-left, unshaded region S_{a}. The upper panels show standard equilibrium points (saddle, focus, node), which lend their names to the corresponding canard points shown in the lower panels (folded saddle, folded focus, folded node). The difference between the upper and lower panels is the direction of the trajectories on S_{r} due to the parametrization, $\bar{z}$ or z. A folded saddle admits two trajectories through it, along the stable and unstable manifolds of the corresponding saddle. A folded focus does not admit any trajectories. A folded node admits a *funnel* (dotted region) of trajectories between the stronger stable (or unstable) manifold of the corresponding node and F, which follow the weaker stable (or unstable) manifold. This is an adaptation of Figure 10 in [68].

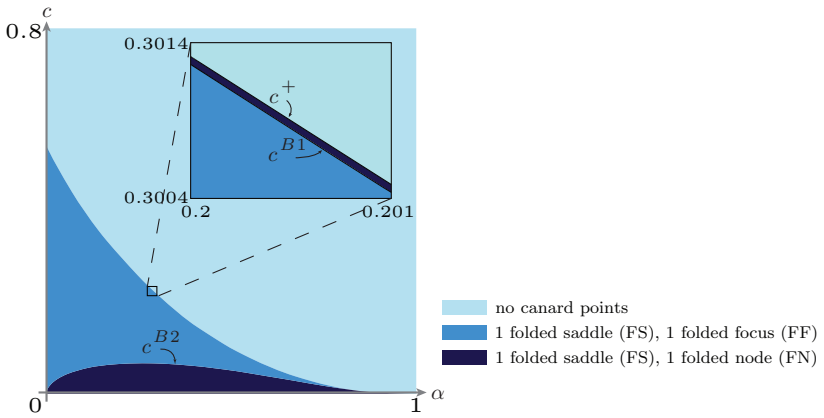

Figure 4.6: The type of canard points of (4.18), in the (α, c)-plane. The canard points are created in a saddle-node bifurcation as c decreases through $c = c^+(\alpha)$, defined in (4.20). The folded node becomes a folded focus at $c = c^{\mathrm{B1}}(\alpha)$ and a folded node once again at $c = c^{\mathrm{B2}}(\alpha) < c^{\mathrm{B1}}(\alpha)$.

We determine the type of the canard points by numerically computing the the eigenvalues of the corresponding equilibria of (4.19). Since the canard points are created in a SN bifurcation, we observe a folded saddle (FS) and a folded node (FN) near the bifurcation point, $c = c^+(\alpha)$. Just after the SN bifurcation, at $c = c^{\mathrm{B1}}(\alpha) < c^+(\alpha)$, the FN becomes a FF (while the FS remains a FS). The FF transitions back to a FN at $c = c^{\mathrm{B2}}(\alpha) < c^{\mathrm{B1}}(\alpha)$; see Figure 4.6. While $c^+(\alpha)$ is determined analytically, and defined in (4.20), $c^{\mathrm{B1,B2}}(\alpha)$ are determined numerically[6].

Lemma 4.3.4. *For $0 < \alpha < 1$ and $0 < c < c^+(\alpha)$, with $c^+(\alpha)$ defined in* (4.20), (4.18) *admits a solution trajectory connecting* $(0, 1)$ *to the FS.*

Proof. For $0 < \alpha < 1$ and $0 < c < c^+(\alpha)$, Lemma 4.3.3 implies that (4.18) has two canard points, $(u_{\mathrm{FS}}, w_{\mathrm{FS}})$ and $(u_{\mathrm{F}}, w_{\mathrm{F}})$, with $\alpha < w_{\mathrm{F}}, w_{\mathrm{FS}} < 1$. It is straightforward to show that the FS, $(u_{\mathrm{FS}}, w_{\mathrm{FS}})$, is the canard point with the larger w-component. Since F corresponds to a monotonically decreasing function of w as u increases, $u_{\mathrm{FS}} < u_{\mathrm{F}}$. Consequently, $(u_{\mathrm{FS}}, w_{\mathrm{FS}})$ lies above and to the left of $(u_{\mathrm{F}}, w_{\mathrm{F}})$ in the (u, w)-phase plane. From (4.18) it follows that $u' > 0$ for $w, c > 0$ and that $w' < 0$ along $w = w_{\mathrm{F}}$ for $0 < u < u_{\mathrm{F}}$. Consequently,

[6]In principle, it may be possible to determine $c^{\mathrm{B1,B2}}$ analytically: the canard points correspond to roots of (4.21) and these roots are a subset of the roots of a quartic polynomial. However, these expressions are so complicated they offer little insight

the trajectory leaving $(0, \alpha)$ does not connect to $(u_{\mathrm{FS}}, w_{\mathrm{FS}})$. Since the u-axis is repelling, it intersects F below and to the right of $(u_{\mathrm{F}}, w_{\mathrm{F}})$. The w-nullcline connecting $(0, 1)$ with the FS is strictly decreasing and the stable eigenvector of the FS lies below that nullcline for $u \lessapprox u_{FS}$. As a result, there is a trajectory leaving $(0, 1)$ that connects to $(u_{\mathrm{FS}}, w_{\mathrm{FS}})$. □

This solution trajectory (that leaves $(0, 1)$, connects to $(u_{\mathrm{FS}}, w_{\mathrm{FS}})$ and, hence, continues onto S_{r}) is the canard solution, which we label T_{o}. It is the only solution trajectory of (4.18) that (partly) lives on S_{r} and connects to $(0, 1)$.

In the remainder of this chapter, we do not consider regimes where FNs are present: $0 < c < c^{\mathrm{B2}}$ and $c^{\mathrm{B1}} < c < c^{+}$. Although we expect that our results are valid for $0 < c < c^{+}$, the analysis of FNs is beyond the scope of this chapter.

Remark 4.4. In the case $\beta = 0$, the u-equation of (4.9) is of first order. In this case, u_z is simply $\frac{u^2 w}{c}$ and the singularly perturbed system becomes three-dimensional.

$$\begin{aligned} u_z &= \frac{u^2 w}{c}, \\ v_z &= -w(1-w)(w-\alpha), \\ \varepsilon w_z &= v - cw + \frac{u^2 w^2}{c}. \end{aligned} \tag{4.22}$$

Consequently, the layer problem becomes one-dimensional, but the defnition of S and the symmetry it has around the fold curve F remain unchanged. Hence, the reduced system and the slow behavior are independent of β, and for $\beta = 0$ are described by (4.18). This is also supported by the simulations of the full PDE system with $\beta = 0$, see Figure 4.7 which has identical parameter values as Figure 4.2, besides $\beta = 0$. The case $\beta = 0$ applies to tumors of which the dominant mechanism of cell migration is haptotaxis rather than chemotaxis, like some solid tumors.

4.3.4 Proof of Theorem 4.3.1

Traveling wave solutions (TWSs) are identified in the four-dimensional phase space of (4.11) or (4.12) as heteroclinic connections between the equilibria

$$(u, v, p, w) = (0, c, 0, 1) \quad \text{and} \quad (u, v, p, w) = (u_\infty, 0, 0, 0).$$

To leading order, flow in the four-dimensional phase-space can be represented by concatenations of the fast flow of (4.13) with u, v constant, describing the TWSs around the shock, and the slow flow of (4.17), describing the TWSs away from the shock. This *glueing together* of solution segments from (4.13) and (4.17)

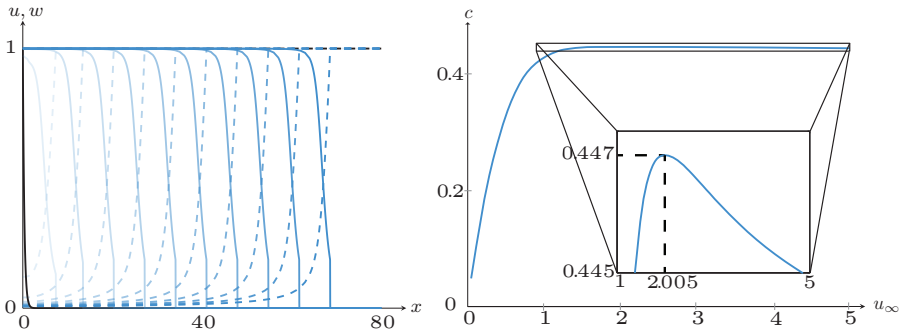

Figure 4.7: Left-hand panel: A *Type III wave* with a biologically justified, well-defined edge and speed $c \approx 0.43$, obtained by numerically simulating (4.1)–(4.2) with $\varepsilon = 0.001$, $\alpha = 0.05$ and $\beta = 0$. The dashed lines correspond to u-profiles and the solid lines to w-profiles, with solutions plotted at $t = 0$ (black), 16 (lightest), $32, \ldots, 160$ (darkest). Note that this is very similar to the left panel of Figure 4.2, because only the fast dynamics is influenced by β, see (4.13). Right-hand panel: The leading order ($\varepsilon = 0$) component of the speed of traveling wave solutions of (4.1)–(4.2) (c) versus the background ECM density (u_∞), with $\alpha = 0.05$, illustrating a biphasic relationship. This is exactly the same as the right-hand panel of Figure 4.2 as the leading order component is independent of β, see (4.18).

is how we construct leading order approximations of TWSs of (4.1)–(4.2). The validation of this approach follows from GSPT and canard theory.

Since both equilibria lie on S_{a}, they both have two-dimensional stable manifolds in (4.13) and a two-dimensional center manifold corresponding to the slow variables. Consequently, a heteroclinic connection cannot be made between the two equilibria purely within (4.13). Similarly, since $(u_\infty, 0)$ in (4.18) has a one-dimensional unstable manifold (since $\alpha > 0$) and a one-dimensional center manifold corresponding to translation in the u-direction, a heteroclinic connection cannot be made between the two equilibria purely within (4.18). Instead, a connection must contain solution segments from both systems. Consequently, no TWSs exist when no canard points are present ($c > c^+(\alpha)$) and TWSs of (4.1)–(4.2) can only be Type III waves since the final part of the heteroclinic connection for $\varepsilon = 0$ has to be a trajectory of (4.13).

According to Lemma 4.3.2 and (4.16), the fast flow is directed from S_{r} to S_{a} and the w-component is symmetric in F, while the u-component is constant. Hence, a heteroclinic connection to $(u_\infty, 0, 0, 0)$ on S_{a} via (4.13) must *take-off* from $(u_\infty, 0, 0, c^2/u_\infty^2)$ on S_{r}. The canard solution is the only solution of the slow flow that (partly) lives on S_{r} and that connects to S_{a} in backward z. So, to construct a heteroclinic connection between $(0, c, 0, 1)$ and $(u_\infty, 0, 0, 0)$, we need the canard solution (in four-dimensional space) to intersect $(u_\infty, 0, 0, c^2/u_\infty^2)$. In the original, (u, w)-coordinates, this means that the canard solution of (4.18) (T_{o}) must intersect the *jump curve*: $J := c^2/u_\infty^2$. In Figure 4.8, the phase plane of (4.18) and J are shown for particular values of α and c; T_{o} and J intersect, yielding a heteroclinic connection of (4.9)–(4.10) with $\varepsilon = 0$ and, hence, a Type III TWS of (4.1)–(4.2) with $\varepsilon = 0$.

With $\varepsilon > 0$, the end states $(0, 1)$ and $(u_\infty, 0)$ do not perturb. Geometric singular perturbation theory implies that the (invariant) manifolds S_{a} and S_{r} perturb to the $\mathcal{O}(\varepsilon)$-close, locally invariant manifolds $S_{\mathrm{a},\varepsilon}$ and $S_{\mathrm{r},\varepsilon}$, respectively, provided S_{a} and S_{r} are normally hyperbolic and ε is sufficiently small. Along F, S loses normal hyperbolicity. However, canard theory guarantees that T_{o} persists [167].

If the unstable manifold of $(0, 1)$ and the stable manifold of $(u_\infty, 0)$ have a transverse intersection for $\varepsilon = 0$, the heteroclinic connection for $\varepsilon = 0$ persists as a solution of (4.9)–(4.10) with $0 < \varepsilon \ll 1$. This condition is equivalent to J and T_{o} intersecting transversally. In D, we show that this *transversality condition* holds, provided $c \neq u_\infty\sqrt{\alpha}$. Hence, a TWS that is constructed for $\varepsilon = 0$, persists as a TWS of (4.1)–(4.2), with $0 < \varepsilon \ll 1$ sufficiently small, provided $c \neq u_\infty\sqrt{\alpha}$, with the former providing a leading order approximation of the latter.

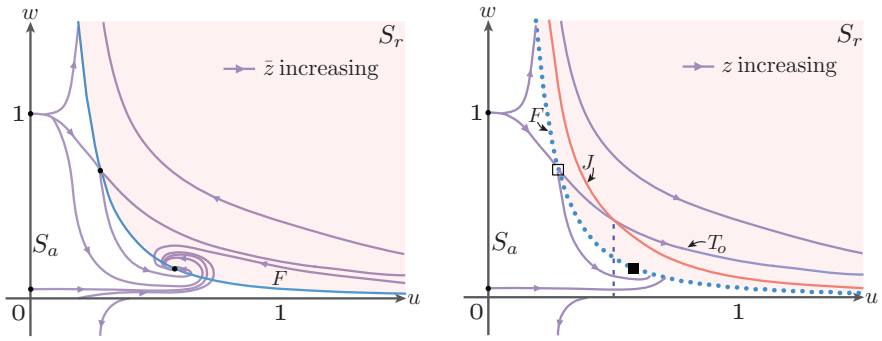

Figure 4.8: Phase planes of (4.19) (left) and (4.18) (right), for $\alpha = 0.05$ and $c = 0.33$. The blue line is the fold curve (F), which is dotted on the right to illustrate its singularity. Black dots represent equilibria. The black open square is a folded saddle and the solid black square is a folded focus. F divides S into a repelling side (S_r, shaded) and an attracting side (S_a, not shaded). The canard solution is labelled T_o (take-off). The curve J given by $w = J(u) = c^2/u^2$ and is a reflection of the u-axis in F. An intersection between J and T_o determines the u_∞ for which a Type III traveling wave solution (with speed c) exists. Here, only one intersection exists.

4.4 Implications of the strong Allee effect

In the previous section, we introduced the mathematical framework to study invasive tumor fronts, or traveling wave solutions (TWSs), of the strong Allee model (4.1)–(4.2) with $0 \lessapprox \alpha < 1$, $0 \leq \beta \leq 1$ and $0 \leq \varepsilon \ll 1$ sufficiently small) connecting the all-cancer state $(0, 1)$ and the cancer-free state $(u_\infty, 0)$ with $u_\infty \in \mathbb{R}^+$. It was shown, in a mathematically rigorous way, that the strong Allee model cannot admit Type I, II or VI TWSs (see Theorem 4.3.1); only TWSs where the w-component has a well-defined edge–Type III waves–can exist. This result is due to the stability of the states $(u_\infty, 0)$. While Type III waves are the only possible TWSs of the strong Allee model, their existence is not guaranteed. In Section 4.3, we derived a condition for the existence of Type III waves.

In this section, we establish the main results presented in Section 4.1.3. We demonstrate the existence of Type III TWSs in the strong Allee model and investigate the relationship between their speed and the background ECM density (u_∞), for different values of ε. We also make a qualitative comparison between the results for the strong Allee model and results for the logistic model, (4.1) with (4.3), [67] and the competition model, (4.1) with (4.4), [108], and review the impact of the inclusion of the strong Allee effect.

4.4.1 Existence of invasive tumor fronts with well-defined edges

Type III TWSs of the strong Allee model exist if a transverse intersection between two specific curves in the phase plane of the ODE system

$$\begin{aligned} u_z &= \frac{u^2 w}{c}\,, \\ \left(c - \frac{2u^2 w}{c}\right) w_z &= -w(1-w)(w-\alpha) + \frac{2u^3 w^3}{c^2} \end{aligned} \tag{4.23}$$

exists; see Section 4.3 for the derivation of this condition. The two curves are the so-called *canard solution*, denoted T_o in Figure 4.9, and the so-called *jump curve*, denoted $J \coloneqq c^2/u^2$ in Figure 4.9. Here, u and w still represent the ECM and cancer cell densities, c is the invasion speed of the tumor and $z = x - ct$ is a new variable–the so-called *traveling wave coordinate*–that corresponds to a coordinate frame moving along with the TWS. Note that (4.23) can also be obtained from the strong Allee model by setting $\varepsilon = 0$ and looking for stationary solutions in the z-coordinate frame.

A consequence of the requirement of an intersection between the canard solution and the jump curve is that no TWSs exist for c greater than a critical value, $c = c^+(\alpha)$, defined in (4.20), as the canard solution does not exist in this regime; see Section 4.3. The behavior of c^+ as a function of α is shown as the

transition curve between the light and dark green regions in Figure 4.6, which shows that $c^+(\alpha)$ is a decreasing function of the Allee threshold α. Tumors requiring a larger threshold to grow, therefore have a slower maximum speed potential. Henceforth, we only consider speeds $c^{\mathrm{B2}}(\alpha) < c < c^{\mathrm{B1}}(\alpha) < c^+(\alpha)$, where $0 < c \leq c^{\mathrm{B2}}(\alpha)$ and $c^{\mathrm{B1}}(\alpha) \leq c < c^+(\alpha)$ are narrow regions where the mathematical analysis becomes more involved and is beyond the scope of this chapter. The analytic expression $c^+(\alpha)$ hence yields an upper bound on the speed of the invading waves. Consequently, the model does not support traveling waves that go faster than this upper limit. So, the expression $c^+(\alpha)$ can be used as a crude measure to give an upper bound on how far an invading wave has traveled at any time without any significant computation. Because $c^+(\alpha)$ is decreasing, a larger α gives a lower upper bound on the speed.

With $c^{\mathrm{B2}}(\alpha) < c < c^{\mathrm{B1}}(\alpha)$, the canard solution is the only solution trajectory of (4.23) that leaves the all-cancer state $(0, 1)$ and crosses the so-called *fold curve*, denoted $F \coloneqq c^2/2u^2$ in Figure 4.9. (This fold is a projection in two dimensions of the fold F of the critical manifold as shown in Figure 4.4). Other trajectories leaving $(0, 1)$ also hit the fold curve, but do not cross it due to the singular nature of (4.23); at the point where the canard solution crosses the fold curve both the left- and right-hand sides of the second equation in (4.23) vanish. This point is a *folded saddle canard point* (FS).

A TWS of the strong Allee model corresponds (to leading order in ε) to the canard solution until it intersects the jump curve, at say $(u, w) = (u_*, c^2/u_*^2)$, at which point it jumps to $(u_\infty, 0)$. This jump corresponds to a shock in the w-component of the (leading order) TWS that connects to zero, while the u-component stays constant ($u = u_*$), creating a Type III TWS with cancer-free state $(u_\infty, 0) = (u_*, 0)$ and speed c (to leading order); see Figure 4.9. The length of the shock is c^2/u_*^2, which is double the distance between the u-axis and the fold curve at $u = u_*$. In other words, the jump curve is the reflection of the u-axis around the fold curve.

Figure 4.9 provides an example phase plane of (4.23) for given α and c, and a schematic of the Type III TWS that the strong Allee model admits for this parameter set. The fold curve is indicated by the green dotted line. The solid blue lines are solution trajectories of (4.23) and the unique solution trajectory crossing the fold curve (the canard solution) is labelled T_{o}. Potential shocks are indicated by the the dashed blue lines. Due to the symmetry of the shock, the length of the dashed blue lines is twice the distance between the canard solution and the fold curve and the given u-coordinate. Since $(u_\infty, 0)$ are repelling equilibrium points of (4.23), trajectories of (4.23) cannot connect to the u-axis as $z \to \infty$. Consequently, only shocks landing exactly on the u-axis create TWSs; such TWSs are Type III TWSs.

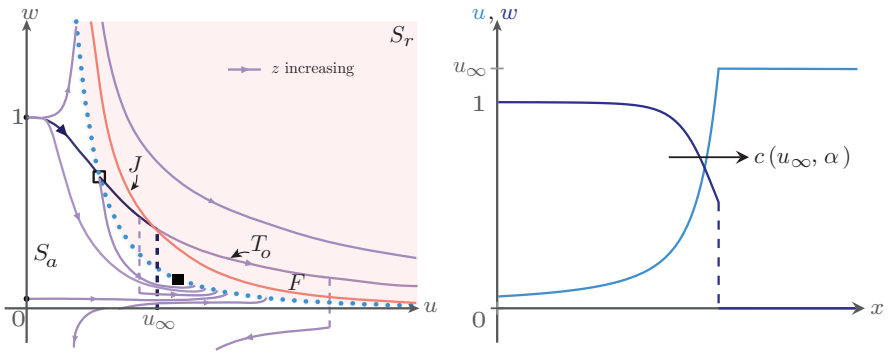

Figure 4.9: Left-hand panel: An example phase plane of (4.23), with $\alpha = 0.05$ and $c = 0.33$. The green dotted line represents the fold curve, labelled F, and the open black square represents the folded saddle, at which the canard solution, labelled T_{o}, crosses the fold curve. The solid blue lines correspond to trajectories of (4.23) and the dashed blue lines correspond to shocks. The jump curve, labelled $J := c^2/u^2$, is shown in orange. A Type III traveling wave solution of the strong Allee model exists since the jump curve and the canard solution intersect transversally. The solid black square is a folded focus canard point, which does not play a role in the construction of traveling wave solutions. Right-hand panel: An illustration of the Type III traveling wave solution (as a function of x) that is obtained from the dark blue trajectory in the phase plane.The w-component has semi-compact support and $u_\infty > 1$ is chosen arbitrarily.

The connection to the u-axis occurs if and only if $u_* = u_\infty$; only if the canard solution intersects the jump curve is a Type III TWS created. The jump curve is indicated by the orange curve in Figure 4.9. For the given parameters, there is a unique intersection between the canard solutions and the jump curve. Therefore, with $\alpha = 0.05$, the strong Allee model admits a unique Type III TWS that travels with speed $c = 0.33$ and asymptotes to the cancer-free state $(u_\infty, 0) = (u_*, 0)$ (to leading order).

4.4.2 Biphasic relationship between invasion speed and background ECM density

In the previous section, we discussed how Type III traveling wave solutions (TWSs) are created. However, several questions remain:

1. For a given α and c, does an intersection between the canard solution and the jump curve always exist, such that a Type III TWS is created?
2. If such an intersection exists, is it unique?
3. Can different speeds yield TWSs that asymptote to the same cancer-free state $(u_\infty, 0)$ with α fixed?

The first question is answered Section 4.3 and discussed in the previous section. For $c > c^+(\alpha)$, there is no canard solution and, thus, no TWSs exist. However, neither Section 4.3 nor the previous section guarantee that the required intersection exists for $c^{\mathrm{B2}}(\alpha) < c < c^{\mathrm{B1}}(\alpha) < c^+(\alpha)$, despite the canard solution existing in this regime. An investigation of the phase portraits of (4.23) for different values of α and c provides further insight into this, and the other questions. The results are presented in Figure 4.10, where the (leading order) speed of the Type III TWS c (if such a TWS exists) is indicated, for the chosen values of α and u_∞.

Figure 4.10 suggests that there is an upper limit $c = c^{\mathrm{trans}}(\alpha)$ on the values of c for which there exists an intersection between the canard solution and the jump curve. This upper limit appears to be less than $c^{\mathrm{B1}} < c^+(\alpha)$ and satisfies the transversality condition derived in D. Consequently, the corresponding value of $u_\infty = u_\infty^{\mathrm{trans}}$ is related to c^{trans} via $c^{\mathrm{trans}} = \sqrt{\alpha} u_\infty^{\mathrm{trans}}$. Moreover, for fixed α, different values of c yield different u_∞-values and it appears that TWSs to all cancer-free states $(u_\infty, 0)$ can be constructed. For a given α, the relationship between the invasion speed of the tumor (c) and the background ECM density (u_∞) has a single turning point–a maximum–at $u_\infty = u_\infty^{\mathrm{trans}}(\alpha)$ with speed $c^{\mathrm{trans}} = \sqrt{\alpha} u_\infty^{\mathrm{trans}}$. This *biphasic* relationship qualitatively resembles experimental results for malignant tumor invasion reported in [125], where the relationship between the collagen concentration and invasion distance of HT1080 is measured

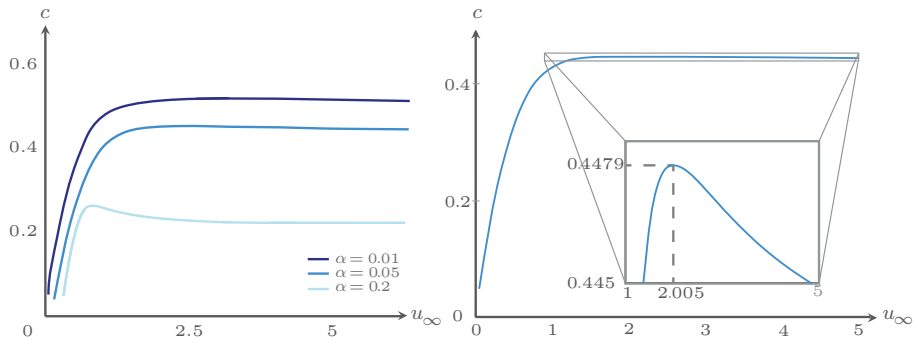

Figure 4.10: Left-hand panel: The leading order speed of the invasive tumor fronts as a function of the background ECM density, for $\alpha = 0.01, 0.05, 0.2$. For increasing α, the *biphasic relationship* between c and u_∞ becomes more prominent and the wavespeed for a given u_∞ decreases. Right-hand panel: A close-up of the $\alpha = 0.05$-curve in the left-hand panel, highlighting the biphasic relationship.

to be non-monotonic. Moreover, the non-monotonicity becomes more pronounced as α increases. Consequently, there is no intersection between the canard solution and the jump curve for $c > c^{\text{trans}}$, and, therefore, no TWS. For $c < c^{\text{trans}}$ there is a narrow region where two intersections exist, which implies the existence of two TWSs, with different end states, that travel with identical speed. However, since the relationship between u_∞ and c illustrated in Figure 4.10 is a graph over u_∞, each background state $(u_\infty, 0)$ corresponds to a single invasion speed. Hence, for a given α and u_∞, we obtain a unique TWS. Figure 4.10 indicates that for increasing α and for fixed u_∞, this speed decreases.

4.4.3 ODE versus PDE

The phase plane and wave shape illustrated in Figure 4.9 as well as the wavespeed results presented in Figure 4.10 are for the strong Allee model with $\varepsilon = 0$. However, provided we are not near the turning point of the biphasic relationship, where transversality between the canard solution and the jump curve is lost, the shape and speed of these traveling wave solutions (TWSs) are good approximations of TWSs of strong Allee model with $0 < \varepsilon \ll 1$; see Section 4.3.4. It is probable that even near the turning points, the $\varepsilon = 0$-solutions are good approximations of the $\varepsilon > 0$-solutions. The location of the turning point will simply shift. However, further mathematical analysis is required to confirm this.

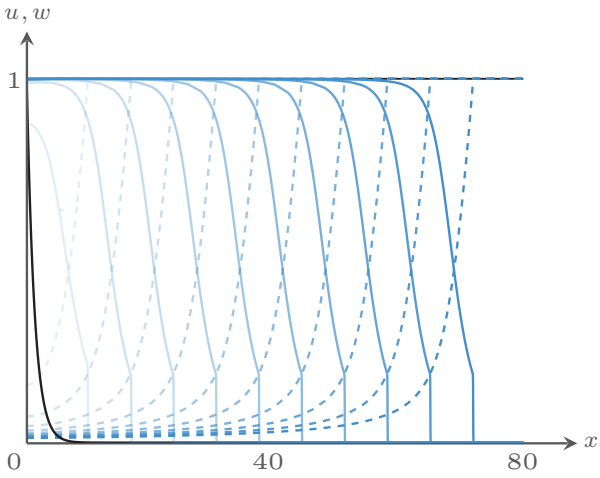

Figure 4.11: A numerical simulation of (4.1)–(4.2), with $\alpha = 0.05$, $\beta = 0.5$, $\varepsilon = 0.001$, $u_\infty = 1$ and a measured speed $c \approx 0.43$, consistent with the ODE results. The dashed lines correspond to u-profiles and the solid lines to w-profiles, with solutions plotted at $t = 0$ (black), 16 (lightest), $32, \ldots, 160$ (darkest).

Figure 4.11 provides an example simulation of (4.1), the strong Allee model with $\varepsilon > 0$, away from the turning point. This simulation shows the evolution of a Type III wave with a speed that agrees with that predicted by the phase plane analysis, to $\mathcal{O}(\varepsilon)$. The figure also suggests that the invasive tumor front is stable, in the sense that it is observable in the system. The initial conditions for this particular simulation are $(u, w) = (u_\infty, \mathrm{e}^{-x})$. However, the same invasive tumor front, with the same speed, appears to evolve from any exponentially decaying w-initial condition, or a w-initial condition with semi-compact support.

Figure 4.12 depicts the results of further numerical simulations for a range of ε and u_∞ values, $\alpha = 0.05$ and $\beta = 0.5$; the right-hand panel is a close-up of the left-hand panel. The solid curve is the biphasic relationship for $\varepsilon = 0$ and $\alpha = 0.05$, given in Figure 4.10. The markers indicate the measured speed of the Type III TWS that evolves from the numerical simulation of strong Allee model, with $\varepsilon > 0$ as indicated. These results demonstrate that for a given u_∞ and α, the invasion speed is an $\mathcal{O}(\varepsilon)$ perturbation of the $\varepsilon = 0$-speed, as expected; see Section 4.3.4. Moreover, they suggest that near the maximum of the solid curve, Type III TWSs continue to exist for $\varepsilon > 0$ with speeds close to the $\varepsilon = 0$-speed.

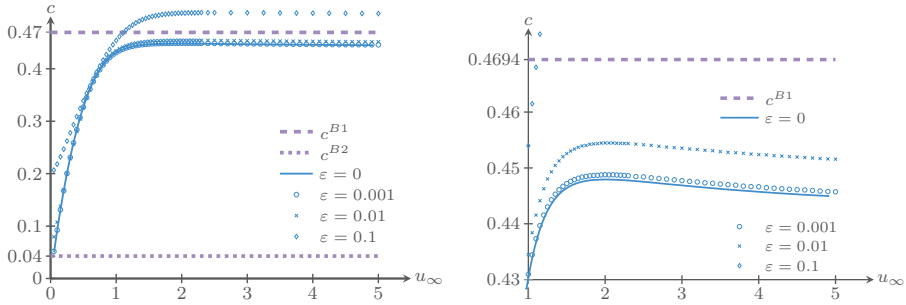

Figure 4.12: The relationship between u_∞ and the measured speed c for Type III traveling wave solutions obtained by numerically simulating (4.1)-(4.2) with $\alpha = 0.05$, $\beta = 0.5$ and ε as indicated, together with bifurcation values of c for $\alpha = 0.05$; see Section 4.3.3. The solid curve indicates the relationship between u_∞ and c for Type III traveling wave solutions with $\alpha = 0.05$ and $\varepsilon = 0$, given in Figure 4.10. The right-hand panel is a close-up of the left-hand panel. The biphasic relationship is clearly visible for small ε.

This observation supports our previous claim that while the mathematical analysis breaks down near the maximum, the results are not significantly altered.

The light blue dashed and dotted curves in Figure 4.12 are values of c at which the phase plane of (4.23) changes qualitatively, for $\alpha = 0.05$; see Figure 4.6. For c values between these lines, the folded focus canard point (FF) denoted by the filled black square in Figure 4.9, remains a FF. The values of c between the light blue dashed and dotted curves ($c^{\mathrm{B2}}(\alpha) < c < c^{\mathrm{B1}}(\alpha)$) represent the regime analysed mathematically in Section 4.3. Thus, we require that for a given α, u_∞ is chosen in such a way that the resulting TWS has a speed in this regime. Based on Figure 4.12, for $\alpha = 0.05$, the minimum value of u_∞ appears to be less than 0.05 (the smallest value we tested). Since $c^{\mathrm{trans}} < c^{\mathrm{B1}}$, there does not appear to be an upper bound on u_∞. The $c^{\mathrm{B1,B2}}$ lines will perturb for $\varepsilon > 0$, which may affect the range of appropriate choices of u_∞. However, the appearance of qualitatively similar TWSs of the strong Allee model for a range of ε values suggests that our analysis remains valid for reasonably large ε values (say, $\varepsilon = 0.1$).

4.4.4 Comparison with models with logistic growth

In this section, we make a qualitative comparison between the strong Allee model and the logistic ((4.1) with (4.3)) and competition ((4.1) with (4.4)) models. The logistic model, where cancer cell growth is modeled by a logistic growth term, is

studied extensively in [67]. The competition model, where a term representing the competition for space between the ECM and cancer cells is appended to a logistic growth term, is studied in [108]. The results of the previous sections, for the strong Allee model, differ from those derived previously, in two main aspects.

For the logistic and competition models, there exists a range of traveling wave solutions (TWSs) with different speeds for a given background ECM density, varying from Type I–IV. This is in contrast to the unique TWS for the strong Allee model. Moreover, this unique TWS is of Type III, the most biologically relevant type, and appears to be stable in the sense that this kind of TWS is observed in numerical simulations of the PDE system, for a wide range of initial conditions. In contrast, for both the logistic and competition models all the Type I–III TWSs appear to be stable. See, for example, Figure 1 in [67] where stable Type I–III TWSs are shown.

The biphasic relationship observed experimentally in malignant tumor invasion [126], occurs in the competition model [108, fig. 10] but not in the logistic model. For the logistic model, the relationship between the invasion speed of the Type III waves and the background ECM density is monotonically increasing [67, fig. 11]. Thus, we conclude that the relationship between u_∞ and c has changed qualitatively due to the Allee effect, in comparison with logistic growth.

4.5 Discussion and future work

In this chapter, we proposed, what is to our knowledge, one of the first model of malignant tumor invasion that explicitly includes Allee effects, [17]. The analysis and results lead us to the conclusion that this model, with the strong Allee effect, is a better model of types of malignant tumor invasion in which hapto- or chemotaxis is the dominant mechanism of cell migration than similar, previously studied models: the logistic model [67, 109, 126] and the competition model [108]. This conclusion is based on the strong Allee model's ability to replicate experimentally observed features of malignant tumor invasion more effectively than the previous models. In particular, the two main results that lead to this conclusion are:

1. The strong Allee model only admits Type III waves, the most biologically relevant invasive tumor fronts, rather than the whole family of Type I–IV waves that is admitted by the logistic and competition models.

2. The relationship between the invasion speed of these Type III waves and the background ECM density is biphasic, which is consistent with experimental observations, contrary to the corresponding relationship for the logistic model.

The results for the weak Allee model are less impressive; see Appendix B. They lead to the conclusion that the weak Allee model is similar to the logistic or competition models as a model of malignant tumor invasion. It admits the same family of traveling wave solutions, including those that are not biologically relevant, and does not exhibit the experimentally justified biphasic relationship between the speed of the Type III waves and the background ECM density.

4.5.1 Additional biological processes

The kinetic function for the cancer cells that we study is a general representation of a cubic function with zero constant term, negative cubic term and positive quadratic term:

$$f_{\text{Allee}}(\hat{w}) = -k_1\hat{w}^3 + k_1(k_2+k_6)\hat{w}^2 - k_1k_2k_6\hat{w} =: K_1\hat{w}^3 + K_2\hat{w}^2 + K_3\hat{w}\,, \quad (4.24)$$

with $K_1 < 0$ and $K_2 > 0$. Thus, appropriate modifications to the second equation in (4.6) (in the form of linear, quadratic or cubic terms in $\hat{w}$) can be expressed and studied using (4.1)–(4.2); the interpretation of the parameters simply changes. Consequently, the results of the Allee model apply more generally and we may use them to infer the effects of including (appropriate) additional biological processes to (4.6).

For example, the death of the cancer cells as a result of treatment or therapy can be modeled by the linear death term $-k_7\hat{w}$, with $k_7 > 0$ (s^{-1}). Appending this term to the $\hat{w}$-equation of (4.6) yields

$$\begin{aligned} \frac{\partial\hat{u}}{\partial\hat{t}} &= -k_4\hat{u}^2\hat{w} + D_1\frac{\partial^2\hat{u}}{\partial\hat{x}^2}\,, \\ \frac{\partial\hat{w}}{\partial\hat{t}} &= k_1\hat{w}(k_2-\hat{w})(\hat{w}-k_6) - k_7\hat{w} - k_3\frac{\partial}{\partial\hat{x}}\left(\frac{\partial\hat{u}}{\partial\hat{x}}\hat{w}\right) + D_2\frac{\partial^2\hat{w}}{\partial\hat{x}^2}\,. \end{aligned} \quad (4.25)$$

Upon applying the nondimensionalisation

$$u_{\text{d}} = \frac{\hat{u}}{U_{\text{d}}}\,, \quad w_{\text{d}} = \frac{\hat{w}}{W_{\text{d}}}\,, \quad t_{\text{d}} = \frac{\hat{t}}{T_{\text{d}}}\,, \quad x_{\text{d}} = \frac{\hat{x}}{X_{\text{d}}}\,, \quad (4.26)$$

with

$$\begin{aligned} U_{\text{d}} &= \frac{k_1}{k_4}W_{\text{d}}\,, \quad W_{\text{d}} = \frac{1}{2}\left(k_2+k_6+\sqrt{(k_2-k_6)^2-4\frac{k_7}{k_1}}\right)\,, \\ T_{\text{d}} &= \frac{1}{k_1W_{\text{d}}^2}\,, \quad X_{\text{d}} = \sqrt{\frac{k_3}{k_4W_{\text{d}}}}\,, \end{aligned}$$

and

$$\alpha_{\mathrm{d}} \coloneqq \frac{k_2 + k_6}{W_{\mathrm{d}}} - 1\,, \quad \beta_{\mathrm{d}} \coloneqq \frac{D_1}{D_2} = \beta\,, \quad \varepsilon_{\mathrm{d}} \coloneqq \frac{k_4}{k_1 k_3 W_{\mathrm{d}}} D_2\,,$$

and dropping the subscript d, (4.25) transforms to the Allee model, (4.1)–(4.2). We assume $k_7 < k_7^* = k_1(k_2 - k_6)^2/4$ so that W_{d} is real-valued.

To interpret the effect of the additional death term, we analyse how the dimensionless variables and parameters change between (4.7) and (4.26), keeping the remaining dimensional parameters k_i, $i \in \{1, 2, \ldots, 6\}$ fixed. The death rate k_7 appears directly in W_{d} and indirectly via W_{d} in the other terms (excluding $\beta_{\mathrm{d}} = \beta$). It is straightforward to see that a death rate k_7 decreases W_{d} compared to W: $W_{\mathrm{d}} < W$. Consequently,

$$U_{\mathrm{d}} < U\,, \quad T_{\mathrm{d}} > T\,, \quad X_{\mathrm{d}} > X\,, \quad \alpha_{\mathrm{d}} > \alpha\,, \quad \beta_{\mathrm{d}} = \beta\,, \quad \varepsilon_{\mathrm{d}} > \varepsilon\,.$$

As expected, the expression for W_{d} corresponds to the background state of (4.25) that represents the carrying capacity of the cancer cell density; the cancer cell density in (4.2) has been scaled to one so the *representative* cancer cell density $W_{[.]}$ used in the nondimensionalisation must correspond to this background state. In terms of their relationship to W_{d}, the other quantities in the nondimensionalisation remain unchanged.

The parameter α_{d} represents the ratio of the two nontrivial w-background states of (4.25), consistent with α in (4.2). Consequently, for $\alpha_{\mathrm{d}} > 0$, this parameter still imposes a growth threshold. However, in terms of the dimensional variables, the growth threshold is no longer represented by $k_6 > 0$ but by $k_6 + k_7/(k_1 k_2) > 0$. Increasing k_7 causes the two nontrivial $\hat{w}$-background states of (4.25) to approach each other on the $\hat{w}$-axis, until they collide and become complex-valued at $k_7 = k_7^*$. In (4.2), since the greater background state is scaled to one, increasing k_7 increases the value of the lesser nontrivial $\hat{w}$-background state, which has been scaled to α. Consequently, to obtain results for (4.25) we take $\alpha < \alpha_{\mathrm{d}} < 1$ (with $\alpha_{\mathrm{d}} \to 1$ as $k_7 \to k_7^*$). As evidenced by Figure 4.10, for $\alpha > 0$, increasing α causes an overall decrease in the speed of the waves. Thus, adding a linear death term to the strong Allee model slows the invasive tumor fronts.

On more speculative terms we may conclude that, as incorporating a growth threshold yields a better match between experimental data and model data, cancer treatment may be improved. If indeed tumor cells cannot survive when the density is low, therapy only needs to be applied until the density is below this threshold. If more experimental data would be available, these thresholds can be determined.

4.5.2 Shortcomings and future work

In this chapter, we proposed a model of malignant tumor invasion that we argue is an improvement on previously studied models of its kind. However, our proposed model is still far from a complete description of malignant tumor invasion; any mathematical model describing a biological process is highly simplified. It it rarely possible to identify the exact mechanisms that are involved in a given process and parameter values such as reaction-rates are often only known to several orders of magnitude. Even if the biology is completely understood, it remains a challenge to represent it mathematically in a way that is both accurate and manageable. For example, irregularities in the border of malignant tumors can be important [3, e.g.], contributing to the speed and severity of the tumor. However, to capture these irregularities, two- or three-dimensional models must be used. Such models are highly complex and not conducive to rigorous mathematical analysis. In the quickly developing field of cancer research, the correct formulation of a model is an ongoing debate. We chose to model the Allee effect with the cubic function (4.2). However, other functional forms may also be used; see, for example, [25] and references therein. Nevertheless, simple models, such as the Allee model, still provide useful information. In this case, we demonstrate that using the strong Allee effect instead of logistic growth has strong implications on the modelling of malignant tumor invasion. They also provide a stepping stone towards understanding more realistic, complex models.

The mathematical methods in this chapter focus on proving the existence of traveling wave solutions. Although the PDE simulations provide an indication of which of these solutions are stable, a rigorous stability analysis remains to be undertaken. One method of inferring stability results for models such as (4.1) is based on an Evans function computation. Such a method is at the time of publishing under development; see [69]. A related aspect that is not discussed in this chapter is the *transient dynamics* of the traveling wave solutions. We do not discuss how an initially small, localised patch of cancer cells evolves into an invading tumor front or how the cancer cells come to be present in the first place. Instead, we investigate the possible long term behaviors of pre-existing tumors. An alternative model is necessary to describe the early stages of tumor development; the prime feature of the strong Allee effect is the growth threshold it imposes, which causes populations less than the threshold value to become extinct. The stability and transient dynamics of the traveling wave solutions studied here are topics for future research.

Finally, our analysis is only valid for sufficiently small values of ε. The numerical simulations suggest that our results remain (at least qualitatively) sound for quite large values of ε, say, $\varepsilon = 0.1$ (see, for example, Figure 4.12). However, we purposely avoid specifically defining *sufficiently small* as this goes

beyond the scope of this chapter. An investigation of the effect of larger ε is left for future research.

Appendices

A Logistic growth and the Allee effect

To gain an understanding of the influence of the Allee effect, in comparison to logistic growth, consider the two ordinary differential equations (ODEs)

$$\frac{\mathrm{d}w}{\mathrm{d}t} = f_{\text{logistic}}(w) = w(1-w) \quad \text{and} \quad \frac{\mathrm{d}w}{\mathrm{d}t} = f_{\text{Allee}}(w) = w(1-w)(w-\alpha)\,. \tag{4.27}$$

Both ODEs are separable and can be solved analytically; sketches of the solutions are given in Figure A.1. The ODEs with logistic growth and the weak Allee effect yield growth (or decay) to the dimensionless carrying capacity ($w = 1$) for any positive initial condition. In contrast, the ODE with the strong Allee effect yields growth (or decay) to the dimensionless carrying capacity only if an initial condition is greater than the threshold value $\alpha > 0$; initial conditions less than $\alpha > 0$ result in the extinction of the species. The differences between logistic growth and the strong and weak Allee effects are further explained by looking at the *per capita growth rate* (pcgr) of w, in the absence of spatial (or other) effects. The pcgr of w is defined as

$$\text{pcgr}(w) \coloneqq \frac{1}{w}\frac{\mathrm{d}w}{\mathrm{d}t} = \frac{\mathrm{d}(\log w)}{\mathrm{d}t}\,,$$

where $\log w$ represents the natural logarithm of w. We determine the pcgr of w for the two cases, logistic and Allee, using $\mathrm{d}w/\mathrm{d}t$ defined in (4.27):

$$\text{pcgr}_{\text{logistic}}(w) = 1 - w\,, \quad \text{pcgr}_{\text{Allee}}(w) = (1-w)(w-\alpha)\,.$$

Figure A.2 provides an illustration of these curves for $w \geq 0$.

For $0 < \alpha < 1$, the pcgr curve for the strong Allee effect is negative in a neighbourhood of $w = 0$, before becoming positive at $w = \alpha$. This negativity, which corresponds to negative population growth, characterizes the strong Allee effect. For $-1 < \alpha < 0$, the pcgr curve for the weak Allee effect decreases almost everywhere except for a small increasing part for $w \in [0, (1+\alpha)/2)$. This increase characterizes the weak Allee effect.

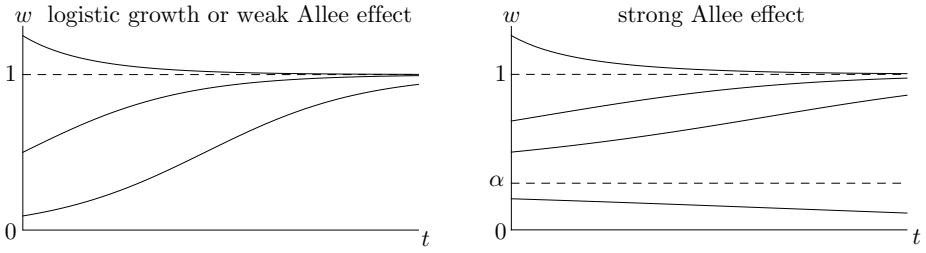

Figure A.1: Sketches of the solutions to the ODEs in (4.27). Left-hand panel: The OD]Es with logistic growth and the weak Allee effect yield growth (or decay) to the carrying capacity (scaled to one) for all positive initial conditions. Right-hand panel: The ODE with the strong Allee effect only yields growth to the carrying capacity for initial conditions larger than the threshold value $\alpha > 0$. Initial conditions smaller than $\alpha > 0$ result in the extinction of w.

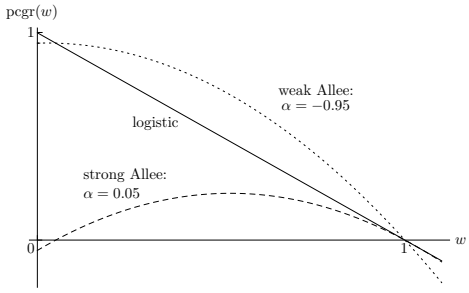

Figure A.2: The pcgr curves for logistic growth (solid), the strong Allee effect (dashed) and the weak Allee effect (dotted). The negativity of the dashed curve for $w < \alpha$ characterizes the strong Allee effect. The turning point in the dotted curve at a *small* value of w relative to the carrying capacity (in this case, at $w = 1/40$), combined with the positive intercept (at $w = 0$), characterizes the weak Allee effect.

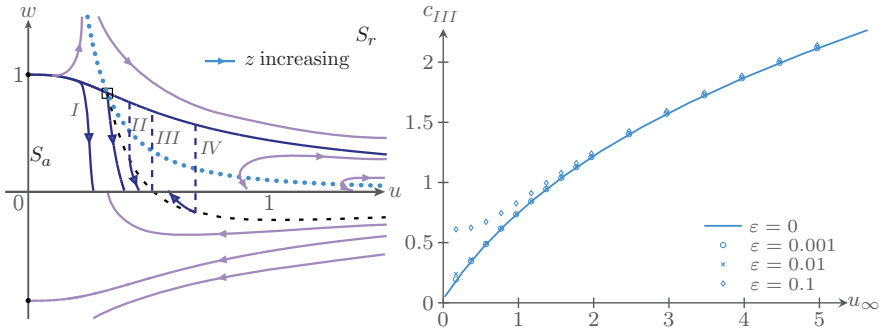

Figure B.1: Left-hand panel: Phase plane of (4.18), parametrized by z, with $\alpha = -0.95$, $c = 0.43$. The green line is the fold curve (F), which is dotted to illustrate its singularity. Black dots represent equilibria. The black open square is a folded saddle. F divides S into a repelling side (S_{r}, shaded) and an attracting side (S_{a}, unshaded). There exist a family of heteroclinic connections corresponding to Type I–IV traveling wave solutions. Right-hand panel: The relationship between the background ECM density (u_∞) and the speed of a Type III wave (c_{III}), with $\alpha = -0.95$. The solid curve is obtained from ODE simulations of (4.19); the markers are obtained from PDE simulations of the weak Allee model.

B Results for the weak Allee model

The mathematical techniques outlined in Section 4.3 can be directly applied to the weak Allee model ((4.1)–(4.2) with $\alpha \gtrapprox -1$). With $\alpha < 0$, the equilibrium $(u, w) = (0, \alpha)$ lies on the negative w-axis and the equilibria $(u_\infty, 0)$ are center stable, in constrast to the case presented in Section 4.3 with $\alpha > 0$. This means that the phase planes of the reduced problem in the weak and strong cases differ considerably, especially near the u-axis. In the weak case, trajectories can approach $(u_\infty, 0)$ via either the fast or slow dynamics, instead of only the fast. For $|\alpha|$ sufficiently large (see Remark 4.5), one canard point exists on F: a folded saddle. The left-hand panel of Figure B.1 illustrates these features and depicts an example phase plane for the weak Allee model.

The configuration of canard points and end states $(u_\infty, 0)$ for the weak Allee model is equivalent to that of the logistic model. Consequently, the analysis of the former is very similar to the latter, which is described in detail in [67]. By glueing together trajectories of the reduced and layer problems, as in Section 4.3.4, we construct a family of Type I–IV traveling wave solutions, parametrized

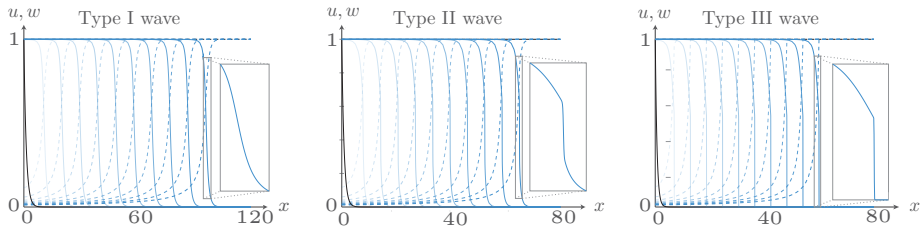

Figure B.2: Type I–III waves with speeds $c \approx 1.2, 0.80$ and 0.73, respectively, obtained by numerically simulating (4.1) with $\varepsilon = 0.001$, $\alpha = -0.95$ and $\beta = 0.5$. The only imposed difference between the three simulations is the initial condition, in particular, the steepness of the w-component; steeper w-components lead to slower waves. The dashed lines correspond to u-profiles and the solid lines to w-profiles, with solutions plotted at $t = 0$ (black), 8 (lightest), $16, \ldots, 80$ (darkest).

by c, for a given u_∞ and $\varepsilon = 0$. The Type III waves correspond to solutions that approach $(u_\infty, 0)$ via the fast dynamics, similar to the Type III waves in the strong Allee model. The Type I, II and IV waves correspond to solutions that approach $(u_\infty, 0)$ via the slow dynamics.

The persistence of these solutions follows from geometric singular perturbation theory and canard theory, using very similar arguments to those presented in [67]. One difference arises from a *transversality condition*, which is automatically satisfied in the logistic model but is violated in the weak Allee model if $u_- = u_+ = c/\sqrt{1+\alpha}$, where $u_\pm$ is the u-coordinate of the shock; see Section 4.3.2. The full implications of this loss of transversality remain to be determined. One immediate implication is the breakdown of the proof of persistence for $0 < \varepsilon \ll 1$ for any traveling wave solutions that violate the transversality condition. Another implication appears to be the existence of nonunique solutions, that is, two possible traveling wave solutions for a given α, c, u_∞ and $\varepsilon = 0$: one with a shock and one without. Numerical simulations of the weak Allee model with $0 < \varepsilon \ll 1$ suggest that the Type I–III waves are stable; see Figure B.2.

The right-hand panel of Figure B.1 provides a plot of the speed of the Type III waves c_{III} as a function of the background ECM density u_∞, for fixed $\alpha = -0.95$. This monotonically increasing relationship resembles the corresponding relationship for the logistic model, rather than the experimentally justified biphasic relationship.

Remark 4.5. The above discussion of the weak Allee effect requires $|\alpha|$ to be sufficiently large. This is ensure that there exists exactly one canard point on F. For $-7 + 4\sqrt{3} \approx -0.072 < \alpha < 0$, there may exist three canard points on

F, depending on the value of c. As c increases, the number of canard points on F changes from one to three and back to one via two saddle-node bifurcations. Although this regime may be mathematically interesting, it is not biologically relevant since the weak Allee effect requires $\alpha \gtrapprox -1$; see A. Consequently, we do not consider it here.

C Dimensionless variables and parameters

$$
\begin{aligned}
[u] &= [\hat{u}]\frac{[k_4]}{[k_1][k_2]} = \frac{\mathrm{kg}}{\mathrm{m}^3} \times \frac{\mathrm{m}^6}{\mathrm{kg} \times \mathrm{cells} \times \mathrm{s}} \times \frac{\mathrm{cells} \times \mathrm{s}}{\mathrm{m}^3} = 1 \\
[w] &= [\hat{w}]\frac{1}{[k_2]} = \frac{\mathrm{cells}}{\mathrm{m}^3} \times \frac{\mathrm{m}^3}{\mathrm{cells}} = 1 \\
[x] &= [\hat{x}]\sqrt{\frac{[k_2][k_4]}{[k_3]}} = \mathrm{m} \times \sqrt{\frac{\mathrm{cells}}{\mathrm{m}^3} \times \frac{\mathrm{m}^6}{\mathrm{kg} \times \mathrm{cells} \times \mathrm{s}} \times \frac{\mathrm{kg} \times \mathrm{s}}{\mathrm{m}^5}} = 1 \\
[t] &= [\hat{t}][k_1][k_2]^2 = \mathrm{s} \times \frac{\mathrm{m}^3}{\mathrm{cells} \times \mathrm{s}} \times \frac{\mathrm{cells}}{\mathrm{m}^3} = 1 \\
[\alpha] &= \frac{[k_6]}{[k_2]} = \frac{\mathrm{cells}}{\mathrm{m}^3} \times \frac{\mathrm{m}^3}{\mathrm{cells}} = 1 \\
[\beta] &= \frac{[D_1]}{[D_2]} = \frac{\mathrm{m}^2}{\mathrm{s}} \times \frac{\mathrm{s}}{\mathrm{m}^2} = 1 \\
[\varepsilon] &= \frac{[k_4]}{[k_1][k_2][k_3]}[D_2] = \frac{\mathrm{m}^6}{\mathrm{kg} \times \mathrm{cells} \times \mathrm{s}} \times \frac{\mathrm{cells} \times \mathrm{s}}{\mathrm{m}^3} \times \frac{\mathrm{kg} \times \mathrm{s}}{\mathrm{m}^5} \times \frac{\mathrm{m}^2}{\mathrm{s}} = 1
\end{aligned}
$$

D Transversality

The curves J and T_o intersect at $(u, w) = (u_\infty, c^2/u_\infty^2)$. Since T_o follows the vector field, this intersection is transverse (not tangent) if

$$
\left.\frac{\mathrm{d}J}{\mathrm{d}u}\right|_{u=u_\infty} - \left.\frac{\mathrm{d}w}{\mathrm{d}u}\right|_{(u,w)=(u_\infty, c^2/u_\infty^2)} \neq 0\,,
$$

where $\mathrm{d}w/\mathrm{d}u$ is the ratio of the ODEs in (4.19). A straightforward computation shows that the above express is given by

$$
\frac{2c^2}{u_\infty^3} + \frac{c^2(1 - c^2/u_\infty^2)(c^2/u_\infty^2 - \alpha) - 2u_\infty^3 c^4/u_\infty^4}{u_\infty^2(2u_\infty^2 c^2/u_\infty^2 - c^2)} = \frac{(u_\infty^2 - c^2)(c^2 - \alpha u_\infty^2)}{u_\infty^6} \neq 0\,.
$$

So, transversality is lost if $c = u_\infty$ or $c = \sqrt{\alpha}\,u_\infty$. The former case implies that the take-off point of the jump is $(u, w) = (c, 1)$, which is only possible if $c = 0$.

Thus, given $u_\infty, c > 0$, transversality is violated only if $c = \sqrt{\alpha}\, u_\infty$. This speed corresponds to a take-off point of the jump at $(u, w) = (u_\infty, \alpha)$.